

Chapter 2

Basic Concepts

The design of laser diodes (LDs) in the group-III-nitride material system follows, in principle, concepts already known from other III–V materials. However, the unique properties of the nitrides introduce certain issues that have to be considered in the fabrication of optoelectronic devices.

This chapter starts with a description of the basic layout of an edge-emitting semiconductor laser and explains the functional layers used in such a device. Based thereon, special characteristics of the nitrides, such as the strong piezoelectric polarization and the large difference in mobility for electrons and holes, are explained with respect to their impact on the design of laser diodes. In particular, issues are covered that arise from the usage of layers with high indium content, which are required to reach an emission wavelength in the green spectral range. The mechanism of optical gain in GaN-based laser diodes is explained together with optical losses and their physical origin. Finally, a simulation model based on laser rate equations is introduced which describes the dynamical properties of laser diodes depending on a set of internal device parameters.

2.1 Double Heterostructure Ridge Laser Diodes

The principal requirements for any laser system are a pump source, an active medium which amplifies light via stimulated emission and a resonator for optical feedback. In a double heterostructure ridge laser diode, a layer structure of different semiconductor materials is used to implement these components. Such devices are grown by means of metal-organic vapor phase epitaxy (MOVPE) or molecular beam epitaxy (MBE). The pump mechanism is given by a current which flows through a p–n junction and creates electrons and holes in the space charge region. These charge carriers are trapped in one or multiple thin layers which have a lower bandgap than the surrounding material, the quantum wells. Population inversion, which is required for stimulated emission to overcome the absorption, can be reached in these quantum wells already at moderate pump current densities.

An optical waveguide is formed in the transversal direction by employing materials with different refractive index. Additionally, index-guiding of the optical mode in the lateral direction is achieved by fabricating a few micrometer wide ridge on top of the laser diode using photo lithography and dry etching. This way, the emitted light is confined in a small volume around the active region, which provides a high photon density in the active region and thereby an enhancement of the stimulated emission. The cleaved facets of the laser diode chip then form a Fabry–Perot resonator, as they reflect a part of the emitted light back to the material, owing to the refractive index contrast between semiconductor and air. The reflectivities of the facets can be altered by applying high-reflective or anti-reflective dielectric coatings.

A dielectric passivation on the areas aside the ridge limits the current flow to the small ridge volume, where the optical mode is confined. This causes a high current density in the range of kA/cm^2 already at a moderate current and prevents a parasitic current flow in regions where there is little or no photon intensity from the optical mode.

Ridge laser diodes in the group-III-nitride material system are conventionally grown homoepitaxially by MOVPE on c-plane oriented free-standing GaN substrate. Although it is possible to grow such devices heteroepitaxially on sapphire [1] or SiC [2], these substrates have severe drawbacks for the manufacturing of laser diodes, namely a high defect-density and a considerable lattice mismatch to GaN. Best laser performance can be achieved by growth on defect-reduced GaN templates, which are fabricated by epitaxial lateral overgrowth (ELOG) on free-standing GaN wafers [3]. In group-III-nitrides, n- and p-type conductivity are enabled by doping with silicon and magnesium, respectively. The availability of n-doped substrates allows for a vertical current path in GaN-based laser diodes. While the activation energy of Si is lower than the thermal energy at room temperature, it is as high as 170 meV [4] for Mg atoms, which makes high Mg-dopant concentrations in the range of 10^{19} cm^{-3} necessary to achieve sufficient p-type conductivity. Self-compensation effects occurring at such high doping levels limit the maximum achievable p-conductivity in MOVPE-grown p-GaN layers to $1.2 (\Omega\text{cm})^{-1}$ [5].

Figure 2.1 shows a schematic drawing of a GaN-based ridge laser diode and its epitaxial structure. The optical waveguide is formed by roughly 200 nm of doped GaN between thicker cladding layers of AlGaIn, which has a lower refractive index. Situated in the center of the waveguide is the active region, which comprises one or multiple InGaIn quantum wells separated by GaN barriers. On the p-side of the active region, a thin AlGaIn layer with a high bandgap is implemented, which acts as an electron blocking layer (EBL) to prevent an overflow of electrons into the p-side. It is separated from the quantum wells by an undoped GaN barrier and an undoped spacer layer. A highly Mg-doped GaN layer on top of the p-cladding enables an ohmic contact to the Ni/Au metal stripe on the ridge and the overlying contact pad. The substrate is thinned down to less than $100 \mu\text{m}$ to facilitate the cleavage of the single chips and an n-contact metal is deposited to the bottom side.

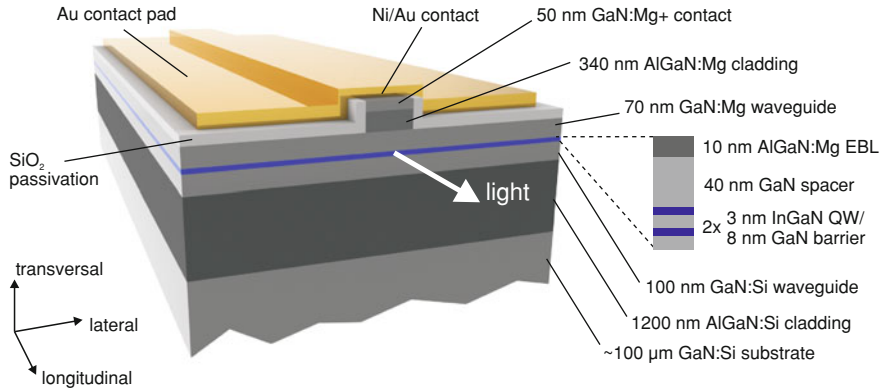


Fig. 2.1 Schematic view of a GaN-based ridge laser diode (not to scale) with description of an example layer structure. The active region is magnified to show the quantum wells

2.2 Heterostructure-Design in Group-III-Nitrides

In order to develop laser diodes which are suitable for applications, tough requirements regarding threshold current, slope efficiency, forward voltage, emission wavelength, output power, and beam quality have to be met. This requires not only a high crystal quality of the epitaxial layers, but also a sophisticated heterostructure design. Particularly in the group-III-nitride system, the width and composition of the individual layers strongly affects the laser performance due to issues that arise from their unique material properties. These issues become even more severe when further developing lasers towards longer emission wavelengths in the green spectral range. The vast number of variation possibilities in a laser diode structure makes it necessary to employ simulation-based concepts for the optimization of heterostructures.

2.2.1 Bandgap and Refractive Index Engineering

The concept of a double heterostructure laser relies on the availability of crystalline materials which differ in bandgap and refractive index, but have a similar lattice constant, so they can be grown pseudomorphically on a common substrate. This allows the growth of optical waveguides and structures that confine the charge carriers, such as quantum wells. Within certain limitations, the ternary alloys AlGaIn, AlInN and InGaIn fulfill this requirement. Their bandgap and refractive index can be tuned over a wide range by varying their composition, as shown in Fig. 2.2. InGaIn is used for the quantum wells. Its bandgap, and thereby the emission wavelength, can be tuned all over the visible spectrum, from near-ultraviolet (GaN) to mid-infrared (InN). Cladding layers for the laser waveguide are typically made of AlGaIn, which has a lower refractive index than GaN. Limitations for the epitaxial design of a

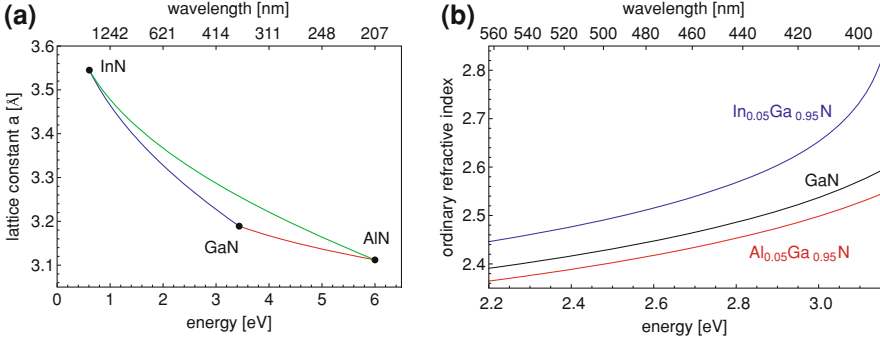


Fig. 2.2 Bandgap and lattice constant a for ternary nitride alloys (a) and refractive index as function of photon energy for $\text{Al}_{0.05}\text{Ga}_{0.95}\text{N}$, GaN and $\text{In}_{0.05}\text{Ga}_{0.95}\text{N}$ (b). Refractive indices are calculated from an analytical model described in Ref. [6]

laser diode are imposed by the lattice mismatch of the alloys to GaN. The critical thickness of a layer, that is the maximum thickness which can be grown before relaxation effects take place, scales with the inverse of the lattice mismatch. It is thus not possible to stack layers of arbitrary thickness and composition. Exceeding the critical thickness of InGa_N leads to the formation of point defects and a rapid deterioration of the optical properties of the layer [7], while for AlGa_N it leads to cracking of the epitaxial layers. This is particularly challenging for green laser diodes, as they require both a high indium content in the active region and thick cladding layers, owing to the reduction of the refractive index contrast of GaN and AlGa_N with increasing wavelength (compare Fig. 2.2b).

In GaN-based laser diodes, the purpose of the optical waveguide is not only to maximize the overlap of the optical mode with the active region, but also to prevent a leakage of the optical mode to the GaN substrate, which can act as a parasitic second waveguide [8]. In order to optimize the waveguide with respect to these two requirements, numerical simulations can be used that solve the scalar wave equation

$$\left(\frac{\partial^2}{\partial y^2} + \frac{\partial^2}{\partial z^2} + n^2(y, z)k_0^2 \right) E(z) = n_{\text{eff}}^2 k_0^2 E(z), \quad (2.1)$$

which is derived from the Maxwell equations [9]. Here, $n(y, z)$ is the refractive index profile, n_{eff} is the effective index of refraction of the optical eigenmode and $k_0 = 2\pi/\lambda$, with the wavelength in vacuum λ . The transversal and lateral directions are z and y , respectively, and x is the (longitudinal) propagation direction. Figure 2.3 shows one-dimensional optical mode simulations for the layer structure presented in Sect. 2.1, with cladding layers containing 5% aluminum, at different emission wavelengths. While at 405 nm, the optical mode is well confined in the waveguide, with a high intensity at the quantum wells and almost none in the substrate, it becomes significantly broader at 510 nm and coupling to a guided mode in the substrate

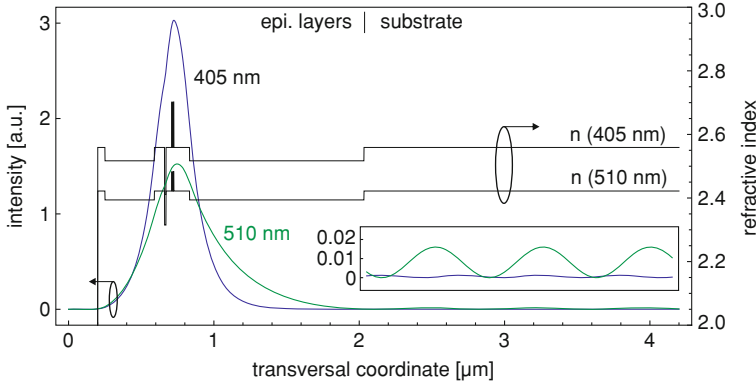


Fig. 2.3 Intensity distribution of optical eigenmodes in the example laser structure shown in Sect. 2.1 at 405 nm (blue) and 510 nm (green) and corresponding refractive index profiles (black). The inset shows a magnification of the intensity distribution in the substrate

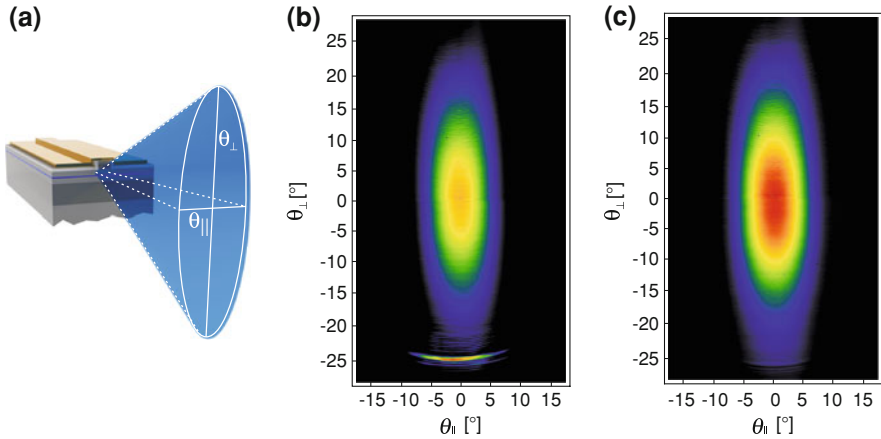


Fig. 2.4 Schematic view of the laser beam (a) and far-field of violet laser diodes with (b) and without (c) a substrate mode peak

occurs. As the far-field of the laser diode is given by the Fourier transform of the optical mode, this substrate mode causes a sharp peak at an angle between 20° and 25° downwards, depending on the effective index of refraction of the laser mode. Insufficient mode confinement also causes an increase in internal optical losses and threshold current [8]. Example far-field patterns of violet laser diodes with different n-claddings, acquired directly with a CCD camera, are shown in Fig. 2.4.

While in violet laser diodes, mode leakage to the substrate can be avoided by using thick claddings with low aluminum content around 5%, this approach becomes increasingly difficult at longer wavelengths. Already in the blue spectral range, the required width of the n-cladding for sufficient substrate mode suppression becomes

several micrometers, due to the reduced contrast of refractive index between GaN and AlGaIn [10]. To avoid substrate modes in green laser diodes and achieve a sufficient beam quality, which is crucial particularly for projection applications, several approaches have been proposed to improve the waveguide: AlInN can be grown lattice matched to GaN and has a much lower refractive index, which makes it well suited as a cladding material [11], although the epitaxial growth of this material with high quality is challenging. Alternatively, InGaIn with low indium content can be used for the waveguide layers to improve the refractive index contrast between waveguide and cladding [12]. Another approach employs a highly n-doped GaN layer below the usual AlGaIn cladding [13]. Owing to the plasmonic effect, this layer has a reduced refractive index and acts as an additional plasmonic cladding layer.

2.2.2 Piezoelectric Polarization and Active Region Design

The active region of a laser diode serves to confine charge carriers in a small volume where they can recombine via spontaneous or stimulated emission or nonradiative mechanisms. For optimum laser performance, the active region must be designed to maximize the stimulated emission and suppress all other recombination channels. The radiative recombination rate is proportional to the wave function overlap, which depends strongly on the width and indium content of the quantum wells in the group-III-nitrides.

In the wurzite phase, which is the stable phase of the group-III-nitrides, these materials exhibit a strong spontaneous and piezoelectric polarization along the *c*-axis, which is commonly the growth direction for GaN-based optoelectronic devices. As the polarization depends on the composition and strain state of the material, discontinuities appear at the interfaces of the epitaxial layers. These discontinuities give rise to internal electric fields due to the Gauss law

$$\vec{\nabla} \cdot (\epsilon \epsilon_0 \vec{E} + \vec{P}) = 0. \quad (2.2)$$

The internal fields tilt the quantum wells, causing a separation of electron and hole wave functions and a reduction of the transition energy, which is known as the quantum confined Stark effect (QCSE). Although the separated charge carriers can partially screen the internal field, the overlap is still drastically reduced at charge carrier densities relevant for laser operation in quantum wells with an indium content greater than 10%. Increasing the indium content in the quantum wells results in higher strain and stronger internal fields. Wide quantum wells leave electrons and holes more space to separate. Therefore, the wave function overlap reduces with increasing indium content or QW width, as shown in Fig. 2.5. On the other hand, an increase of the QW width provides a higher overlap of the active region with the optical mode and improves the optical mode confinement due to the high refractive index of InGaIn. Still, the strong internal fields limit the range of practical QW widths to few nanometers, at least in conventional devices grown on *c*-plane GaN.

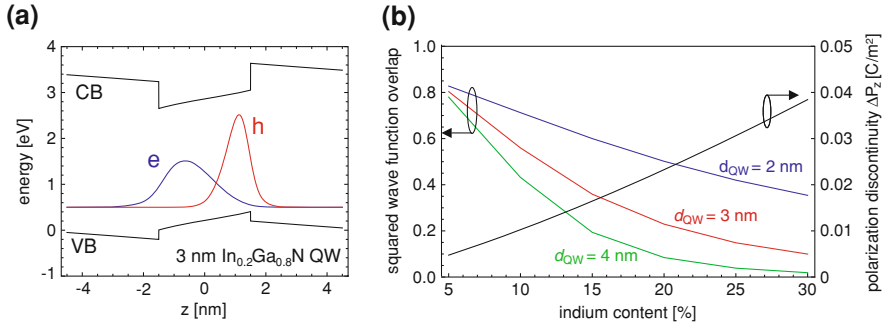


Fig. 2.5 Band profile of a 3 nm In_{0.2}Ga_{0.8}N quantum well with electron and hole probability densities at a charge carrier density of $5 \times 10^{12} \text{ cm}^{-2}$ (a). Squared electron-hole wave function overlap for different quantum well widths and polarization discontinuity as functions of indium content (b)

Determining the optimum number of quantum wells is difficult for nitride laser diodes. The transparency charge carrier density, which has to be pumped into each quantum well before population inversion starts, is rather high in the nitrides, owing to the high effective hole mass [14]. The low mobility of the holes also leads to an inhomogeneous distribution of charge carriers among the wells, especially for deep quantum wells [15]. This makes a high number of quantum wells undesirable. On the other hand, using only a single quantum well implies a very high charge carrier density in the active region, which causes band filling effects [16] and a low charge carrier lifetime that has to be compensated with a higher pump current. Therefore, the number of QWs is typically chosen between one and three [14, 17, 18].

2.2.3 Band Profile and Charge Carrier Transport

Apart from optimizing the active region for stimulated emission, one also has to ensure that injected charge carriers are captured by the quantum wells and do not overshoot past the active region. In the group-III-nitrides, the mobility of holes is one to two orders of magnitude smaller than the electron mobility [4]. This asymmetry in mobilities causes a significant fraction of electrons to leak out of the active region and reach the p-contact metal. To reduce the charge carrier leakage, an electron blocking layer made of high bandgap material, typically AlGaN, is inserted on the p-side in GaN-based optoelectronic devices. To ensure that this layer blocks electrons and not holes, a high p-doping level is required in the vicinity of the EBL [19]. The injection efficiency is given by the fraction of current which goes into the quantum wells, divided by the total current that flows through the device. For shallow quantum wells, it can be analyzed by calculating the current distribution in the device using a drift-diffusion simulation. The simulation has to take into account the field of the p-n junction, the polarization fields arising from heterostructure interfaces and

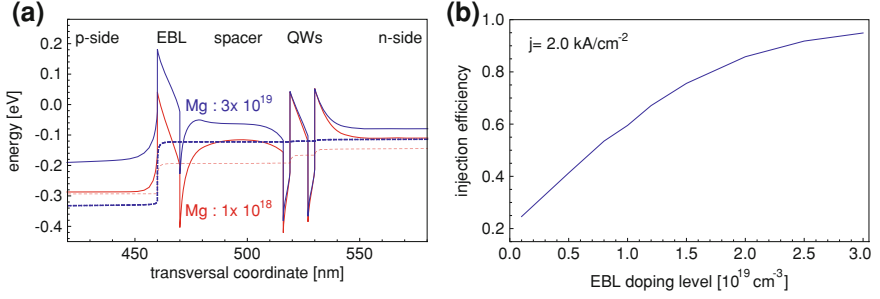


Fig. 2.6 Conduction band profile of the active region and electron blocking layer of a laser diode for Mg doping levels in the EBL of $1 \times 10^{18} \text{ cm}^{-3}$ (red) and $3 \times 10^{19} \text{ cm}^{-3}$ (blue) (a). The dashed lines mark the respective Quasi-Fermi levels. Injection efficiency as a function of EBL doping level at a current density of 2 kA/cm^2 (b)

the screening of internal fields by the charge carrier distribution in a self-consistent way. For deeper quantum wells, which are used for green laser diodes, this quasi-equilibrium approach is no longer a good approximation. In such structures, the quantum mechanical scattering rates between bound states in the quantum wells and propagating carriers have to be calculated [15].

Figure 2.6 shows the conduction band profile of a violet laser diode with two quantum wells and an $\text{Al}_{0.15}\text{Ga}_{0.85}\text{N}$ electron blocking layer, which is calculated using the SiLENSe package [20]. At a low doping level in the EBL, the polarization discontinuity at the heterostructure interface pulls the electron barrier downwards and reduces the effective tunneling barrier for electrons. This reduction cannot be compensated by increasing the aluminum content of the EBL, as a higher aluminum content would also increase the piezoelectric polarization. Instead, the reduction of the barrier can be partly compensated by a high Mg doping level around 2 to $3 \times 10^{19} \text{ cm}^{-3}$ near the EBL. At this doping level, an injection efficiency greater than 90% is achieved at current densities which are typical for laser diodes.

2.3 Band Structure and Optical Gain

The purpose of the active region in a heterostructure laser is to provide optical gain, which amplifies light via stimulated emission. Optical gain is enabled by radiative recombination of electrons and holes from confined states in the quantum wells which have population inversion. To investigate optical gain in a laser diode, it is thus necessary to determine the band structure of the quantum well. Therefore, the 6×6 - $k \cdot p$ method is used, a fast numerical method which calculates the energies and wave functions of electrons and holes in vicinity of the Γ -point [21]. This is sufficient for the modeling of optoelectronic devices, as only these states are populated with charge carriers at the relevant injection currents. The energy bands E_i , E_f and wave

functions $\psi_i, \bar{\psi}_f$ of initial (i) and final (f) states are obtained from a numerical solution of the Schrödinger equations for valence and conduction band

$$\left(\mathbf{H}_h(k_x, k_y, -i \frac{d}{dz}) + V_{VB}(z) \right) \bar{\psi}_f(z) = E_f \bar{\psi}_f(z), \quad (2.3)$$

$$\left(\mathbf{H}_e(k_x, k_y, -i \frac{d}{dz}) + V_{CB}(z) \right) \psi_i(z) = E_i \psi_i(z). \quad (2.4)$$

Here, $V_{VB/CB}$ are the band profile for valence and conduction band, (k_x, k_y) is the in-plane wavevector of the confined charge carriers and the differential operator d/dz is used to implement quantum confinement along the transversal direction. The operator \mathbf{H}_h is a 6×6 effective mass matrix, which accounts for the $P_{x,y,z}$ -angular momentum of the hole states, the anisotropic effective hole masses, the strain potentials and the spin degree of freedom. For the electrons, the effective mass operator \mathbf{H}_e is a scalar, as the electrons are spin degenerate and their angular momentum is S -type. Figure 2.7a shows the band structure of an InGaN quantum well. Three distinct, nearly spin degenerate valence bands occur: The heavy hole (HH), light hole (LH) and crystal field split off (CH) band. Their angular momentum eigenfunctions are $P_x + iP_y$, $P_x - iP_y$ and P_z , respectively. The CH-band is shifted to lower energy due to the relatively large crystal field splitting and a negative strain shift that affects the states which have a hole polarization along to the growth direction. Replicas of these bands appear for the higher order confinement states of the quantum wells. Within the $k \cdot p$ -approximation, the band structure of a wurzite semiconductor has a radial symmetry in the c -plane, so the energy dispersion is identical along the x and y -directions in the quantum well.

Radiative recombination has to fulfill energy and momentum conservation, so the relevant transitions in the band structure are vertical, as the momentum of the photon is much smaller than momentum of the charge carriers. Dipole selection rules determine the optical polarization of the emitted photons. As the hole population, which is given by the Fermi-Dirac function, is highest in the topmost bands, this implies that the emitted photons are predominantly polarized in-plane. Therefore, optical gain occurs only for guided modes with an in-plane polarization, the transversal electric (TE) modes.

Within the free-carrier-theory, the material gain G is calculated from the band structure by summing over all possible transitions, weighted with the transition matrix element and a Fermi factor for the population inversion [22],

$$G(\hbar\omega) = \frac{1}{d} \frac{e^2}{4\pi^2 m_0^2 c_0 \varepsilon_0 n_{\text{eff}} \omega E_{\text{hom}}} \sum_{i,f} \int d^2k \left| M_{if}(\vec{k}) \right|^2 \cdot \text{sech} \left(\frac{\Delta E_{if}(\vec{k}) - \hbar\omega}{E_{\text{hom}}} \right) \left(f(E_i(\vec{k}), \mu_e) - f(E_f(\vec{k}), \mu_h) \right), \quad (2.5)$$

$$M_{if}(\vec{k}) = \langle i | \vec{a} \cdot \vec{p} | f \rangle(\vec{k}), \quad (2.6)$$

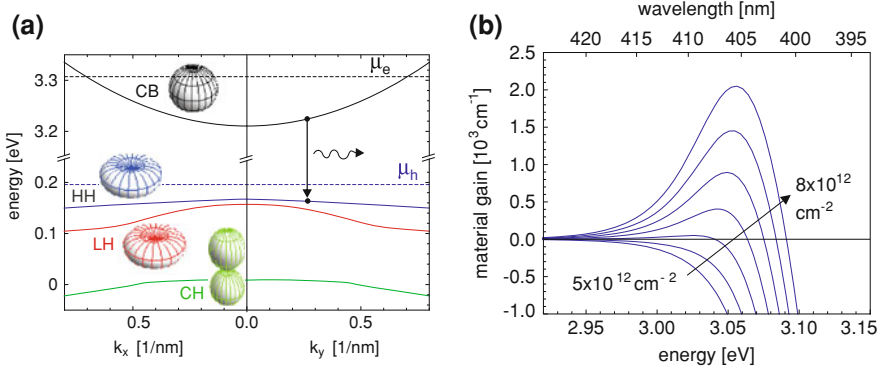


Fig. 2.7 **a** Band structure of a 3 nm $\text{In}_{0.1}\text{Ga}_{0.9}\text{N}$ QW. The insets show the angular momentum eigenfunctions of the individual bands. The dashed lines show the quasi-Fermi levels for electrons (black) and holes (blue) at a charge carrier density of $8 \times 10^{12} \text{ cm}^{-2}$ and room temperature. The arrow marks one possible optical transition. Higher order confinement states appearing between LH and CH band are omitted here for clarity. **b** Homogeneously broadened optical gain spectra calculated from the band structure for charge carrier densities from 5 to $8 \times 10^{12} \text{ cm}^{-2}$ in steps of $0.5 \times 10^{12} \text{ cm}^{-2}$ (bottom to top curve)

$$\Delta E_{if}(\vec{k}) = E_i(\vec{k}) - E_f(\vec{k}). \quad (2.7)$$

Here, d is the quantum well width, m_0 the free electron mass, c_0 the speed of light in vacuum, ϵ_0 the vacuum permittivity, e the elementary charge, $\hbar\omega$ the photon energy and n_{eff} the effective index of refraction of the laser mode. Homogeneous broadening due to charge carrier dephasing is implemented by a sech-function, with a broadening energy of typically $E_{\text{hom}} = 25 \text{ meV}$ [23]. For the simulation of real, imperfect quantum wells, an additional inhomogeneous broadening in the range of 30–100 meV is typically employed [24]. M_{if} is the transition matrix element, with the photon polarization vector \vec{a} , the momentum operator \vec{p} and the electron and hole wave functions i, f . It is proportional to the wave function overlap in the quantum well. The population inversion of the electron and hole states enters via the difference of the Fermi-Dirac functions $f(E_{i/f}, \mu_{e/h})$, with the quasi-Fermi energies $\mu_{e/h}$. The simple free-carrier gain model presented here is sufficient to study qualitatively the dependence of optical gain on the device design. To reach quantitative agreement with experiments, more sophisticated models have to be used that take into account many-body effects [22].

Calculated gain spectra for different charge carrier densities are shown in Fig. 2.7b. At a sufficiently high charge carrier density, positive gain occurs at photon energies close to the effective bandgap, which is given by the bandgap of bulk InGaN plus the strain shift, the confinement energy of the charge carriers and the redshift due to the quantum confined Stark effect. The spectral width of the optical gain is determined by the homogeneous and inhomogeneous broadening and the filling of energetic

states in the band structure. At a photon energy much smaller than the effective bandgap, the gain is zero and there is no absorption by the quantum wells, as no such energetic transitions are available in the band structure. Positive gain is reached only if there are possible transitions in the band structure which have population inversion. The population of a state in a semiconductor is given by the Fermi-Dirac distribution function $f(E, \mu)$, so the condition of population inversion translates into a condition for the transition energy $\hbar\omega$:

$$\underbrace{(1 + \exp(\beta(E_f(k_{tr}) - \mu_h)))^{-1}}_{=f(E_f(k_{tr}), \mu_h)} < \underbrace{(1 + \exp(\beta(E_i(k_{tr}) - \mu_e)))^{-1}}_{=f(E_i(k_{tr}), \mu_e)} \quad (2.8)$$

$$\Rightarrow \mu_e - \mu_h > E_i(k_{tr}) - E_f(k_{tr}) = \hbar\omega$$

with $\beta = 1/(k_B T)$, k_B the Boltzmann constant, T the temperature (which is 300 K in this case), $E_{i/f}(k)$ the conduction and valence band dispersion relations and k_{tr} the transition wavenumber. Optical gain is thus only possible for transitions which fulfill $\hbar\omega < \mu_e - \mu_h$. For energies higher than the difference of the quasi-Fermi levels $\mu_e - \mu_h$, there is no population inversion and the quantum well becomes absorbing.

The material gain can be implemented into a waveguide simulation as the imaginary part of the refractive index of the quantum well layers. The modal gain g of the guided mode is then obtained from the imaginary part of the calculated effective index of refraction. As an approximation, it is also possible to estimate the modal gain as the product of the material gain and the optical confinement factor Γ , which is the overlap integral of the optical mode with the quantum wells:

$$g(\hbar\omega) = \Gamma G(\hbar\omega) = \left(\int_{\text{QWs}} |E(z)|^2 dz \right) G(\hbar\omega) \quad (2.9)$$

In a laser diode waveguide, there is not only optical gain but also losses due to absorption on dopant atoms or crystal defects. For nitride based laser diodes, the dominant loss mechanism is absorption on bound holes from non-ionized acceptors in the p-type layers [25]. The fraction of non-ionized acceptors in these layers is high due to the large acceptor activation energy of the Mg atoms. The optical losses of Mg-doped GaN are 50–100 cm⁻¹ [26]. Therefore it is important to minimize the overlap of the optical mode with p-type layers to achieve low absorption losses [27].

These internal losses are described by an absorption coefficient α_{int} . Another loss mechanism is the transmission of photons through the front and back mirrors. The propagation of a monochromatic electromagnetic wave is described by a complex effective index of refraction n_{eff} ,

$$E(x) = E_0 e^{i n_{\text{eff}} k_0 x}, \quad (2.10)$$

$$n_{\text{eff}} = n_R + i \frac{\alpha}{2k_0}. \quad (2.11)$$

Here, n_R is the real part of the effective index of refraction and α is the extinction or amplification coefficient (depending on whether it is positive or negative). The intensity after one round trip in the laser resonator is:

$$I(2L) = R_1 R_2 I_0 e^{(g(\hbar\omega) + \alpha_{\text{int}})2L}, \quad (2.12)$$

with the front and back mirror reflectivities R_1 and R_2 , the resonator length L , the modal gain $g(\hbar\omega)$ and the internal losses α_{int} . Combining Eqns. 10 to 12 gives the extinction/amplification coefficient α :

$$\alpha = -g(\hbar\omega) + \alpha_{\text{int}} + \underbrace{\frac{1}{2L} \ln(R_1 R_2)}_{\alpha_{\text{m}}}. \quad (2.13)$$

At the laser threshold, the intensity inside the resonator remains constant. The optical gain then just compensates the internal losses α_{int} and the losses of light which is coupled out at the mirrors α_{m} . Therefore, α must become zero, which gives the threshold gain g_{th} :

$$g_{\text{th}} = \alpha_{\text{int}} + \alpha_{\text{m}}. \quad (2.14)$$

To reach a low laser threshold, it is thus necessary to minimize the optical losses in the resonator and to achieve a high optical gain from the quantum wells per injected charge carrier.

2.4 Laser Dynamics

At a sufficiently high pump level, laser operation is enabled by the interaction of the photon field in the cavity and the charge carrier reservoir in the active region of the laser diode. This interaction can be modeled by a system of two coupled differential equations for the charge carrier number N and the photon number S , the rate equations [28]:

$$\frac{dN}{dt} = \frac{\eta_{\text{inj}} I}{e} - \frac{N}{\tau(N)} - g(N, S)cS, \quad (2.15)$$

$$\frac{dS}{dt} = g(N, S)cS + \beta B N^2 - (\alpha_{\text{int}} + \alpha_{\text{m}})cS. \quad (2.16)$$

Here, I is the pump current, η_{inj} the injection efficiency, $g(N, S)$ the modal gain, $c = c_0/n_{\text{gr}}$ the speed of light in the waveguide with the group refractive index n_{gr} , B is the coefficient for spontaneous emission, $\tau(N)$ is the charge carrier lifetime and β the ratio of spontaneous emission into the laser mode, which is estimated as 1×10^{-5} [29].

The notation presented here works with charge carrier and photon numbers instead of densities to keep geometrical factors out of the calculation. The model can be alternatively formulated in terms of area (2D) or volume (3D) densities by scaling the parameters with the active region area or volume. Within this simplified model,

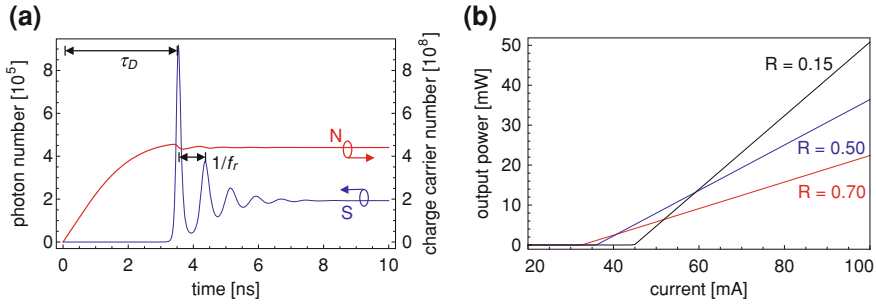


Fig. 2.8 **a** Example time-dependent solution of rate equations for the charge carrier number N and the photon number S for an electrical square pulse starting at $t = 0$. The arrows mark the turn-on delay τ_D and the inverse oscillation frequency $1/f_r$. **b** Simulated output power as a function of pump current for different front mirror reflectivities and a cavity length of $L = 600 \mu\text{m}$

the wavelength dependency of the parameters is neglected and single-mode operation is assumed. Spectral dynamics like mode hopping and multi-mode emission can be implemented by replacing Eq. 2.16 by a set of equations for the individual longitudinal modes with appropriate coupling terms [30].

The dependency of the charge carrier lifetime τ on N can be approximated by the ABC-model

$$\begin{aligned} \frac{N}{\tau(N)} &= R(N) = R_{\text{SRH}} + R_{\text{spont}} + R_{\text{Aug}} = \\ &= AN + BN^2 + CN^3 \end{aligned} \quad (2.17)$$

where the first term relates to Shockley-Read-Hall (SRH) recombination on defects, the second term corresponds to the spontaneous emission and the third term implements Auger recombination. The functional dependence of the modal gain $g(N, S)$ on the charge carrier and photon number can be approximated by a linear model [28],

$$g(N, S) = \frac{dg}{dN} \frac{(N - N_{\text{tr}})}{1 + k_{\text{sat}} S}, \quad (2.18)$$

where dg/dN is the differential gain per carrier number, N_{tr} is the transparency carrier number, and k_{sat} implements gain saturation due to spectral hole burning.

A time-dependent solution of the rate equation model allows to study the dynamical behavior of the laser diode upon turn-on or fast modulation, while the stationary solution yields the dependence of the output characteristics on internal device parameters. Figure 2.8a shows the time evolution of charge carrier number and photon number upon turn-on. After the onset of the electric pulse, there is a turn-on delay τ_D of few nanoseconds during which the active region is filled with carriers up to threshold, then the optical output starts. The laser diode exhibits relaxation oscillations with a frequency f_r and reaches steady state after several nanoseconds. Turn-on

delay and relaxation frequency depend on pump current and on device properties such as the carrier lifetime at threshold and the differential gain. In steady state laser operation, the charge carrier number is clamped to its threshold value and does not depend on the pump current.

Solving Eqs. 2.15 and 2.16 for steady state conditions relates the injection efficiency to the slope of the power-vs.-current curve and the cavity losses

$$\frac{dP}{dI} = \eta_{\text{inj}} \frac{\alpha_m}{\alpha_m + \alpha_{\text{int}}} \frac{\hbar\omega}{e}. \quad (2.19)$$

This provides an accurate method to determine the injection efficiency η_{inj} from measurements of the output power and the internal losses. The influence of the front mirror reflectivity on the output characteristics is shown in Fig. 2.8b. The reflectivity of the rear mirror is set to 1. A high front mirror reflectivity means low mirror losses and therefore a lower threshold current, at the cost of a small slope efficiency dP/dI above threshold. Reducing the mirror reflectivity improves the slope efficiency, as more photons are coupled out of the cavity, but also increases the threshold.

References

1. S. Nakamura, M. Senoh, S.-I. Nagahama, N. Iwasa, Room-temperature continuous-wave operation of InGaN multi-quantum-well structure laser diodes. *Appl. Phys. Lett.* **69**(26), 4056–4058 (1996)
2. S. Bader, B. Hahn, H. Lugauer, A. Lell, A. Weimar, G. Brüderl, J. Baur, D. Eisert, M. Scheubeck, S. Heppel, A. Hangleiter, V. Härle, First european GaN-based violet laser diode. *Physica Status Solidi A* **180**, 177–182 (2000)
3. K. Motoki, Development of gallium nitride substrates. *SEI Tech. Rev.* **70**, 28–35 (2010)
4. J. Piprek, S. Nakamura, Physics of high-power InGaN/GaN lasers. *IEE Proc. Optoelectron.* **149**(4), 145–151 (2002)
5. U. Kaufmann, P. Schlotter, H. Obloh, K. Köhler, M. Maier, Hole conductivity and compensation in epitaxial GaN:Mg layers. *Phys. Rev. B* **62**(16), 867–872 (2000)
6. R. Goldhahn, C. Buchheim, P. Schley, A. Winzer, H. Wenzel, Optical Constants of Bulk Nitrides. In: J. Piprek (eds) *Nitride Semiconductor Devices: Principles and Simulations*, chapter 5 (Wiley VCH, Weinheim, 2007) pp. 95–116
7. D. Queren, M. Schillgalies, A. Avramescu, G. Brüderl, A. Laubsch, S. Lutgen, U. Strauss, Quality and thermal stability of thin InGaN films. *J. Cryst. Growth* **311**(10), 2933–2936 (2009)
8. V. Laino, F. Roemer, B. Witzigmann, C. Lauterbach, U.T. Schwarz, C. Rumbolz, M. Schillgalies, M. Furitsch, A. Lell, V. Härle, Substrate modes of (Al, In)GaN semiconductor laser diodes in SiC and GaN substrates. *IEEE J. Quantum Electron.* **43**, 16–24 (2007)
9. C. Henry, B. Verbeek, Solution of the scalar wave equation for arbitrarily shaped dielectric waveguides by two-dimensional Fourier analysis. *J. Lightwave Technol.* **7**(2), 308–313 (1989)
10. U. Strauss, C. Eichler, C. Rumbolz, A. Lell, S. Lutgen, S. Tautz, M. Schillgalies, S. Brünighoff, Beam quality of blue InGaN laser for projection. *Physica Status Solidi C* **5**(6), 2077–2079 (2008)
11. A. Castiglia, E. Feltin, G. Cosendey, A. Altoukhov, J.-F. Carlin, R. Butte, N. Grandjean, Al_{0.83}In_{0.17}N lattice-matched to GaN used as an optical blocking layer in GaN-based edge emitting lasers. *Appl. Phys. Lett.* **94**(19), 193506 (2009)

12. T. Lermer, M. Schillgalies, A. Breidenassel, D. Queren, C. Eichler, A. Avramescu, J. Müller, W. Scheibenzuber, U. Schwarz, S. Lutgen, U. Strauss, Waveguide design of green InGaN laser diodes. *Physica Status Solidi A* **207**(6), 1–4 (2010)
13. P. Perlin, K. Holc, M. Sarzynski, W. Scheibenzuber, L. Marona, R. Czernecki, M. Leszczynski, M. Bockowski, I. Grzegory, S. Porowski, G. Cywinski, P. Firek, J. Szmidi, U. Schwarz, T. Suski, Application of a composite plasmonic substrate for the suppression of an electromagnetic mode leakage in InGaN laser diodes. *Appl. Phys. Lett.* **95**(26), 261108 (2009)
14. S.-N. Lee, H.Y. Ryu, H.S. Paek, J.K. Son, T. Sakong, T. Jang, Y.J. Sung, K.S. Kim, K.H. Ha, O.H. Nam, Y. Park, Inhomogeneity of InGaN quantum wells in GaN-based blue laser diodes. *Physica Status Solidi C* **4**(7), 2788–2792 (2007)
15. D. Sizov, R. Bhat, A. Zakharian, K. Song, D. Allen, S. Coleman, C. Zah, Carrier transport in InGaN MQWs of aquamarine- and green-laser diodes. *IEEE J. Select. Top. Quantum Electron.* (2011, to be published)
16. W.G. Scheibenzuber, U.T. Schwarz, T. Lermer, S. Lutgen, U. Strauss, Thermal resistance, gain and antiquiding factor of GaN-based cyan laser diodes. *Physica Status Solidi A* **208**, 1600 (2011)
17. D. Queren, A. Avramescu, M. Schillgalies, M. Peter, T. Meyer, G. Brüderl, S. Lutgen, U. Strauss, Epitaxial design of 475 nm InGaN laser diodes with reduced wavelength shift. *Physica Status Solidi C* **4**, 1–4 (2009)
18. S. Uchida, M. Takeya, S. Ikeda, T. Mizuno, T. Fujimoto, O. Matsumoto, T. Tojyo, M. Ikeda, Recent progress in high-power blue-violet lasers. *IEEE J. Select. Top. Quantum Electron.* **9**(5), 1252–1259 (2003)
19. S. Grzanka, G. Franssen, G. Targowski, K. Krowicki, T. Suski, R. Czernecki, P. Perlin, M. Leszczynski, Role of the electron blocking layer in the low-temperature collapse of electroluminescence in nitride light-emitting diodes. *Appl. Phys. Lett.* **90**(10), 103507 (2007)
20. STR Group Ltd., Simulator of Light Emitters based on Nitride Semiconductors (SiLENSe). <http://www.semitech.us/products/SiLENSe>
21. S. Chuang, C. Chang, $k \cdot p$ method for strained wurtzite semiconductors. *Phys. Rev. B* **54**(4), 2491–2504 (1996)
22. S.W. Chow, W.W. Koch, *Semiconductor-Laser Fundamentals* (Springer, Berlin, 1998)
23. B. Witzigmann, V. Laino, M. Luisier, U. Schwarz, H. Fischer, G. Feicht, W. Wegscheider, C. Rumbolz, A. Lell, V. Härle, Analysis of temperature-dependent optical gain in GaN-InGaN quantum-well structures. *IEEE Photonics Technol. Lett.* **18**(15), 1600–1602 (2006)
24. K. Kojima, U.T. Schwarz, M. Funato, Y. Kawakami, S. Nagahama, T. Mukai, Optical gain spectra for near UV to aquamarine (Al, In)GaN laser diodes. *Opt. Express* **15**, 7730–7736 (2007)
25. E. Kioupakis, P. Rinke, C.G. Van de Walle, Determination of internal loss in nitride lasers from first principles. *Appl. Phys. Express* **3**(8), 082101 (2010)
26. M. Kuramoto, C. Sasaoka, N. Futagawa, Reduction of internal loss and threshold current in a laser diode with a ridge by selective re-growth (Ris-LD). *Physica Status Solidi A* **334**(2), 329–334 (2002)
27. U.T. Schwarz, M. Pindl, E. Sturm, M. Furitsch, A. Leber, S. Müller, A. Lell, V. Härle, Influence of ridge geometry on lateral mode stability of (Al, In)GaN laser diodes. *Physica Status Solidi A* **202**(2), 261–270 (2005)
28. K. Petermann, *Laser Diode Modulation and Noise* (Kluwer Academic Publishers, Dordrecht, 1991)
29. L.A. Coldren, S.W. Corzine, *Diode Lasers and Photonic Integrated Circuits* (Wiley, New York, 1995)
30. B. Schmidtke, H. Braun, U.T. Schwarz, D. Queren, M. Schillgalies, S. Lutgen, U. Strauss, Time resolved measurement of longitudinal mode competition in 405 nm (Al, In)GaN laser diodes. *Physica Status Solidi C* **6**, S860–S863 (2009)

GaN-Based Laser Diodes

Towards Longer Wavelengths and Short Pulses

Scheibenzuber, W.G.

2012, XIV, 98 p., Hardcover

ISBN: 978-3-642-24537-4